

This is an Open Access document downloaded from ORCA, Cardiff University's institutional repository: <https://orca.cardiff.ac.uk/id/eprint/107669/>

This is the author's version of a work that was submitted to / accepted for publication.

Citation for final published version:

Kim, Seong-Han, Kim, Teun-Teum, Oh, Sang Soon , Kim, Jae-Eun, Park, Hae Yong and Kee, Chul-Sik 2011. Experimental demonstration of self-collimation of spoof surface plasmons. *Physical Review B: Condensed Matter and Materials Physics* 83 (16) , 165109. 10.1103/PhysRevB.83.165109

Publishers page: <http://dx.doi.org/10.1103/PhysRevB.83.165109>

Please note:

Changes made as a result of publishing processes such as copy-editing, formatting and page numbers may not be reflected in this version. For the definitive version of this publication, please refer to the published source. You are advised to consult the publisher's version if you wish to cite this paper.

This version is being made available in accordance with publisher policies. See <http://orca.cf.ac.uk/policies.html> for usage policies. Copyright and moral rights for publications made available in ORCA are retained by the copyright holders.



Experimental demonstration of self-collimation of spoof surface plasmonsSeong-Han Kim,¹ Teun-Teum Kim,² Sang Soon Oh,³ Jae-Eun Kim,¹ Hae Yong Park,^{1,*} and Chul-Sik Kee^{4,†}¹*Department of Physics, KAIST, Daejeon 305-701, Korea*²*Department of Mechanical Engineering, KAIST, Daejeon 305-701, Korea*³*Department of Physics, Imperial College London, London SW7 2AZ, United Kingdom*⁴*Nanophotonics Laboratory, APRI, GIST, Gwangju 500-712 and Center for Subwavelength Optics, Korea*

(Received 24 January 2011; published 13 April 2011)

We demonstrate experimentally and theoretically that spoof surface plasmons (SSPs) can propagate without diffraction, i.e., self-collimation (SC) of SSPs. To excite and detect SSPs on a structured brass surface, we employed a pair of monopole antennas. The scanned horizontal and vertical field intensity distributions of the SSPs reveal a narrow Gaussian envelope at the SC frequency. While the Gaussian SSP is well maintained, being prevented from spreading during lengthy propagation, SSPs with frequencies below or above the SC frequency diverge. We examine the possibility of steering self-collimated SSPs.

DOI: [10.1103/PhysRevB.83.165109](https://doi.org/10.1103/PhysRevB.83.165109)

PACS number(s): 78.67.Pt, 41.20.Jb, 42.25.Fx, 73.20.Mf

I. INTRODUCTION

Interaction between electromagnetic (EM) waves and coherent fluctuations of electron gas at a metal-dielectric interface creates EM surface waves called surface plasmons (SPs).¹ In optical region, SP fields are strongly confined at the metal-dielectric interface and have decay lengths of subwavelengths. At lower frequencies, in terahertz (THz) and microwave regions, metals also support surface modes known as Zenneck waves on flat surfaces and Sommerfeld waves on cylindrical surfaces.²⁻⁴ Surface modes in THz and microwave regions exhibit very weak confinement, making EM fields reside mostly in the dielectric region because metals can be approximately considered as perfect electric conductors (PECs) into which EM fields cannot penetrate.

However, recent studies⁵⁻¹¹ have shown that PEC surfaces with arrays of subwavelength holes are able to support strongly confined surface modes with SP-like dispersion relations, i.e., spoof surface plasmons (SSPs).^{5,7} Since SSP dispersion relations can be controlled and designed for almost any frequency, SSPs are useful in steering EM waves.¹²⁻¹⁹

Although diffraction occurs with all types of waves, including EM and sound waves, waves may propagate without diffraction within artificial media designed for large anisotropy. Such a phenomenon, or self-collimation (SC), has been observed in artificial periodic structures of dielectric composites, i.e., photonic crystals,²⁰⁻²² or elastic ones, i.e., phononic crystals.^{23,24} Although metal surfaces with two-dimensional (2D) periodic subwavelength holes generate anisotropy in dispersion relations for SPs, researchers have not yet observed SC of SPs due to strong intrinsic absorption by metal surfaces within optical range. Of note, the dispersion relation of SSP is anisotropic for light wavelengths comparable to the period of holes.⁸ Such an anisotropic property possibly allows observation of SC of SSPs,²⁵ opening a new window for steering SSPs from micro- to terahertz waves within a broad spectral range.

In this article, we present both experimental and theoretical demonstrations of the SC of SSPs on a structured brass surface with a periodic array of holes within the microwave range. To predict SC frequency and simulate SC phenomenon near the frequency, we used a 3D finite-difference time-domain

(FDTD) method.²⁶ Further, we employed a pair of monopole antennas to excite and detect SSPs on the sample surface. The scanned horizontal and vertical field intensity distributions of the SSPs revealed a narrow Gaussian envelope at the SC frequency. The width of the Gaussian SSP beam was well maintained, being prevented from spreading during lengthy propagation. Moreover, we observed SSP splitting for frequencies below the SC frequency. Splitting of a SSP beam and subsequent recollimation of each split beam allows the possibility of SSP channeling without employing any special channel structure.

II. PHYSICAL SYSTEM AND NUMERICAL SIMULATION**A. Sample**

The physical system under study was composed of a flat metal plate on which was placed a close-packed square array of hollow square-ended brass tubes with an outer side length, i.e., lattice constant, of $a = 10$ mm, an inner side length, i.e., hole size, of $b = 8.75$ mm, and a hole depth of $h = 40$ mm. Further, $d = \sqrt{2}a$ represents the diagonal length of the unit cell. Figure 1(a) shows the photographic image of the top view of the brass tube array. The cutoff frequency of the lowest waveguide mode of the individual tube was measured to be 17.14 GHz when air is filled. The structure was designed to produce a flat dispersion surface in the frequency range of around 15 GHz for the transverse magnetic- (TM) polarized SSPs.

B. Numerical simulations

The equipfrequency contours (EFCs) for the structured brass surface were obtained via the 3D FDTD method. Bloch periodic boundary conditions were used in the [10] and [01] directions, while perfectly matched layers were placed at the boundaries in the $\pm z$ directions. Since metals in the microwave region are treated as PECs, the brass was modeled as a PEC in this study.

The 45°-rotated magnified views of EFCs for frequencies $f = 0.473$, 0.512, and 0.532 (in units of c/a) are shown in Fig. 1(b), where 'c' is the velocity of light. For $f = 0.512$, the structured brass surface displays almost no spatial dispersion

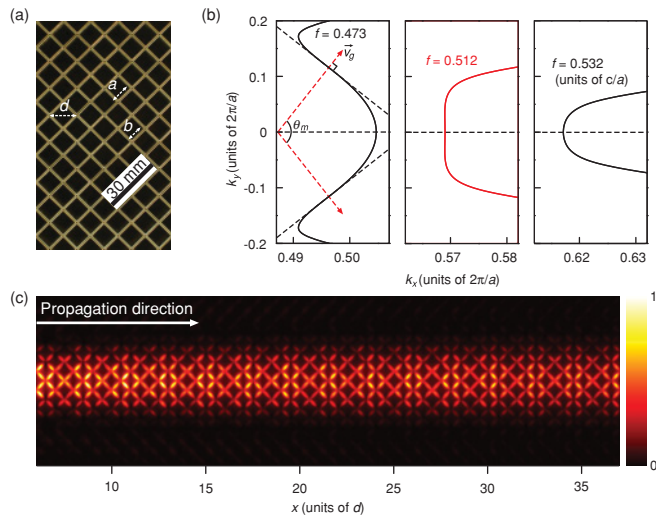


FIG. 1. (Color online) (a) Photographic image of the top view of the array of brass tubes. (b) 45° rotated and magnified views of the EFCs for $f = 0.473, 0.512, 0.532$ (in units of c/a). The maximum angle between the group velocity vector \vec{v}_g and the k_x vector is $\theta_m/2$ in (b). (c) FDTD simulation of self-collimated propagation of a SSP beam at 15.36 GHz.

in the range of the transverse wave vector k_y from -0.04 to 0.04 (in units of $2\pi/a$). Thus, self-collimated propagation of a SSP beam is predicted at $f = 0.512$, i.e., the SC frequency, which is well demonstrated in the FDTD simulation obtained at the SC frequency and displayed in Fig. 1(c). The two flat regions responsible for split propagation of a SSP beam were observed near EFC inflection points for $f = 0.473$, which is below the SC frequency. The maximum angle between the group velocity vector \vec{v}_g and the k_x vector was defined as $\theta_m/2$.

III. EXPERIMENTAL SETUP

Small monopole antennas were employed to generate and detect SSPs. Since a point source generated near-fields with wave vectors of various directions and magnitudes, a small antenna placed near a metal air-holed surface was able to generate SSPs. SSPs on such a surface revealed only TM polarization in which the magnetic field was parallel to the surface, while the loop-shaped electric field extended vertically from the surface.⁷ Therefore, the vertical components of SSP electric fields, as well as those radiated from a vertical monopole antenna, were able to couple very efficiently. Hence, SSP field intensities could be readily measured using a pair of monopole antennas arranged in the vertical direction, as depicted in Fig. 2. The diameter of monopole antennas is 1.6 mm and the length is 10 mm. The detector antenna is mounted on an xyz stage to measure electric field distribution at any given point. The sample is surrounded by a microwave absorber with -20 dB reflectance at normal incidence.

IV. EXPERIMENTAL RESULTS

A. Propagation of SSP beams

SSPs on the structured brass surface were characterized by measuring evanescent electric field intensity within the air

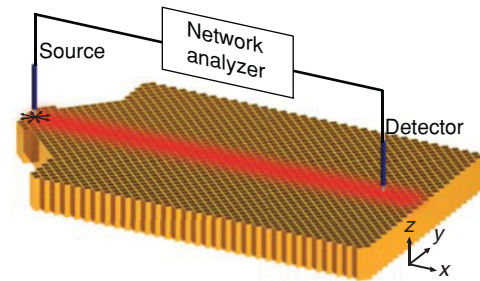


FIG. 2. (Color online) Schematic of an experimental configuration in which two monopole antennas are used to generate and detect the SSPs.

side with two microwave monopole antennas and a network analyzer (Agilent HP8720B). Figures 3(a) and 3(b) show measured and fitted electric field intensities at 15.60 GHz in vertical and horizontal directions, respectively, which are normal to the propagation direction. Of note, the EFCs obtained with the FDTD calculations predicted the SC phenomenon at 15.36 GHz, whereas the SC phenomenon was experimentally observed at 15.60 GHz with about 1.5% difference in the value of the SC frequency. The self-collimated SSP beam decays exponentially in the z direction with a decay constant of 0.649 cm^{-1} . Oscillations in the measured horizontal profile of the electric field along the y direction just above the sample are due to the fact that the fields are strongly confined above the metal region and weakly above the air hole region, on the periodically structured brass surface.⁷ The envelope of the horizontal field intensity profile on the surface displays a narrow Gaussian shape with the beam width of about $3d$, confirming that the SSP beam does not diverge. All these results not only imply that the electric fields are strongly localized at the interface of air and the structured metal but also that the EM power substantially flows along the interface.

To observe the evolution of the SSP beams, we varied the frequency from 13.80 to 16.20 GHz at the interval of 0.012 GHz, measuring the electric field intensity at 73 points in the step of $0.25d$ along the y direction on the $z = 0.5 \text{ mm}$ plane for several values of x . As a result, an electric field intensity distribution was obtained as a 73×401 matrix for each point. Figure 4(a) displays intensity distributions measured on the $z = 0.5 \text{ mm}$ plane as a function of y at $x = 6d, 16d, 26d,$ and $36d$. Such figures elucidate the evolution of SSP beams on the interface and, thus, the varying field intensity distribution in the propagation direction for various frequencies. While SSP beams at the SC frequency propagate effectively without spread, those at frequencies below or above the SC frequency diverge. For comparison, Fig. 4(b) depicts measured SSP beam width for 15.60 and 16.20 GHz as a function of propagation distance. To obtain the beam width, a standard definition of the full width at half maximum (FWHM) is used. During the beam propagation from $x = 6d$ to $x = 36d$, the envelope of intensity profile along the y axis is fitted with a Gaussian curve and the FWHM of self-collimated SSPs for 15.60 GHz increases 4 mm, from 43 to 47 mm, whereas the FWHM obtained for the beam of 16.20 GHz expanded from 57 to 81 mm. For frequencies above the SC frequency, the EFCs have lenslike topology; therefore, the traveling SSP

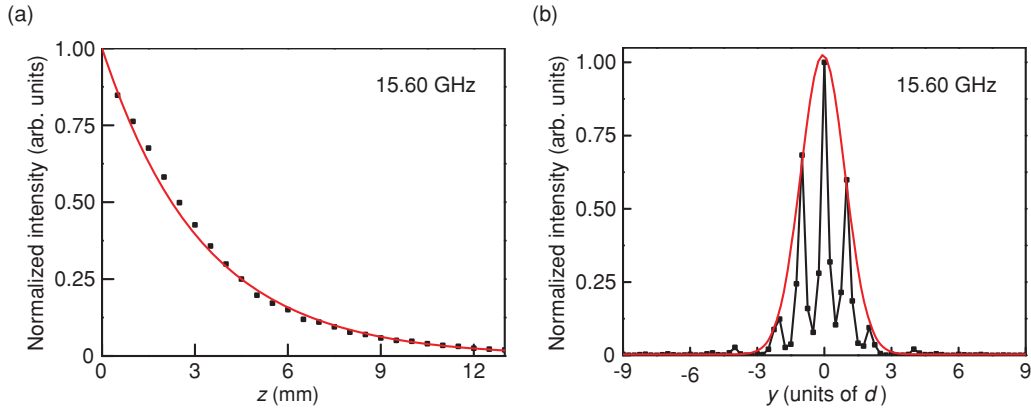


FIG. 3. (Color online) (a) Electric field intensity measured (black dot) and fitted (red line) in the z direction where $x = 16d$ and $y = 0$ at 15.60 GHz. (b) Electric field intensity measured (black dotted line) and Gaussian fitted curve (red line) of the envelope of the measured data in the y direction in the step of $0.25d$ where $x = 16d$ and $z = 0.5$ mm at 15.60 GHz.

beams at those frequencies were expected to have Gaussian profiles with spreading effects. Moreover, Fig. 4(c) shows the intensity profiles of traveling SSPs in the y direction for four different x values at frequencies of 14.40, 15.60, and 16.20 GHz.

B. Propagation loss

Propagation loss, which is an important issue in the application of SSPs, is calculated to be 0.157 dB cm^{-1} from the peak values of beam intensities at $x = 6d$ and $36d$ for the SC frequency of 15.60 GHz, assuming that the shape and width of the wave profiles at the SC frequency remain unchanged. Power loss per one SSP beam wavelength (~ 1.9 cm) at 15.60 GHz was about 0.3 dB. Propagation loss obtained by such a method is meaningless for all SSP frequencies, except the SC frequency, since the beam experiences broadening as it propagates. Scattering via irregular roughness at the interface and also the surface current are deemed to cause the losses.

C. Splitting of a SSP beam

Worth mentioning, SSPs display split propagation into two beams for frequencies below the SC frequency, as shown in Fig. 4(a) [also in the intensity profile obtained at 14.40 GHz in Fig. 4(c)]. Figure 5(a) depicts the measured electric field intensity (black dotted line) at 14.40 GHz where $x = 26d$ and the measured data were fitted with a two-peak Gaussian curve (red line). The vertical lines and numbers in blue denote the peak positions. The two split SSP beams propagate with no appreciable spread. Figure 5(b) displays peak positions y (in units of d) obtained by use of a two-peak Gaussian fitting method (symbols) and linearly fitted (lines) for beams of frequencies of 13.80, 14.10, 14.40, and 14.70 GHz. SSP beam splitting is explained by the existence of two flat regions near the EFC inflection points of the structure at frequencies below the SC frequency, as shown in Fig. 1(b). The divergent angle between the directions in which the two split beams propagate was determined by the angle θ_m , as defined in Fig. 1(b), at the EFC inflection points. As the frequency approaches the SC frequency, θ_m diminishes, and thus the two individual peaks become barely separated. Further, a similar phenomenon occurs in 2D slab photonic crystals, as reported in Ref. 21. The angles between the fitting lines, θ_{fit} in Fig. 5(b), were compared with the values of θ_m . For example, $\theta_{fit} = 28.3^\circ$ and $\theta_m = 28.2^\circ$ for SSP beams at the frequency of 13.80 GHz, while $\theta_{fit} = 15.8^\circ$ and $\theta_m = 14.7^\circ$ for SSP beams at the frequency of 14.40 GHz, displaying good agreement between the two angles.

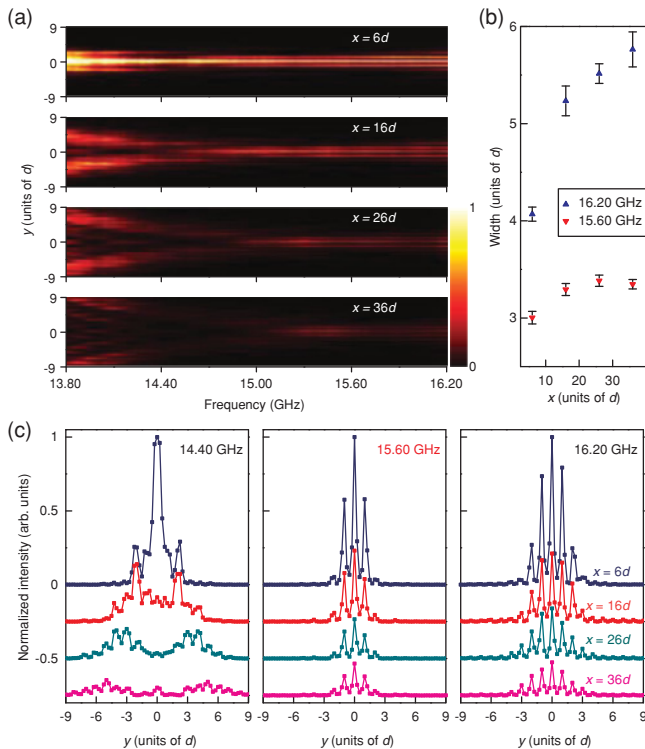


FIG. 4. (Color online) (a) Measured horizontal field intensity distribution of SSPs as a function of frequency on the $z = 0.5$ mm plane where $x = 6, 16, 26,$ and 36 (in units of d). (b) Measured width of SSP beams of 15.60 and 16.20 GHz along the x direction. (c) Measured horizontal field intensity distribution of SSPs where $x = 6, 16, 26,$ and 36 (in units of d) for the frequencies 14.40, 15.60, and 16.20 GHz, respectively, with plots offset by -0.25 increments along the vertical axis.

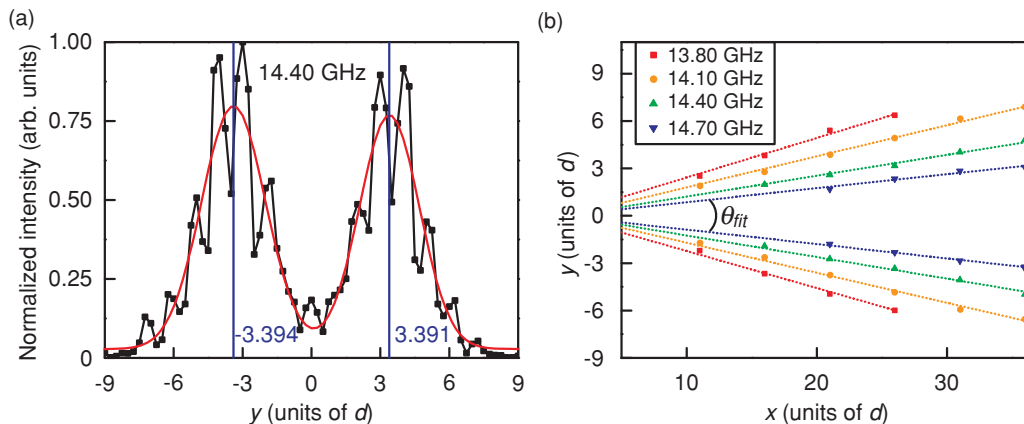


FIG. 5. (Color online) (a) Two-peak Gaussian fitting curve (red line) for the measured electric field intensity (black dotted line) at 14.40 GHz where $x = 26d$. The blue vertical lines and numbers denote the peak positions. (b) The peak positions obtained by the two-peak Gaussian fitting method (symbols) and their linear fitting curves (lines) for the beams of frequencies 13.80, 14.10, 14.40, and 14.70 GHz. θ_{fit} denotes the angle between the fitting lines for 14.70 GHz in (b).

Such splitting phenomena associated with SSP beams could be used in channeling since split SSP beams can be collimated with appropriately designed surface structures. For example, on a structured brass surface with $h = 1.0a$, EFC calculations reveal that the SSP beam at 15.10 GHz collimates when $b = 0.9a$ but splits when $b = 0.7a$. Figure 6(a) shows the simulated field intensity distribution at $z = 0.05a$ of an SSP beam at the frequency of 15.10 GHz on a structured brass surface with two different regions, A and B. A denotes a region with $b = 0.9a$ and B a region with $b = 0.7a$. The self-collimatedly propagating beam in region A splits into two beams in region B. The two split beams exhibit diffraction phenomena, thus spreading out on propagation. Figure 6(b) shows the simulated field intensity distribution obtained at $z = 0.05a$ for the SSP beam at the frequency of 15.10 GHz on the same structured brass surface in which region B is followed

by an additional region A. The two beams split in region B, displaying self-collimated propagation again in the second A region. Though the intensities of the recollimated beams weaken in comparison with those of the initial collimated beam, the simulated results imply that channel SSPs can be realized without any special waveguide structures.

V. CONCLUSION

Possible new designs for the SSP dispersions relation hold the promise of SC frequency control of surface wave propagation on structured metal surfaces. Likewise, the almost perfect conductive properties of conventional metals in the terahertz range inspire us to predict self-collimated propagation of terahertz SSPs as well. In particular, the absence of interaction between intersecting self-collimated SSPs hold possibilities for waveguide application, such as waveguide interconnection with low channel crosstalk in the terahertz range. In addition, SSP beam splitting and subsequent recollimation of each split beam on a structured conductor surface provide the possibility of SSP channeling without introducing any special channel structures. Designing splitters, mirrors, and filters to manipulate self-collimated SSP beam propagation will be undeniably challenging.

In conclusion, we have demonstrated the SC of SSPs on a structured brass surface with a periodic array of holes in microwave range. Moreover, we observed SSP splitting for frequencies below the SC frequency. Our demonstration of diffractionless propagation of SSPs based on the designable dispersion relation is promising in opening new windows for steering SSP propagation, as well as inspiring new ideas for device applications.

ACKNOWLEDGMENTS

This work was supported by the Ministry of Education, Science, and Technology of Korea through the National Research Foundation (2010-0014291, 2010-0001858) and the Ministry of Knowledge and Economy of Korea through the Ultrashort Quantum Beam Facility Program.

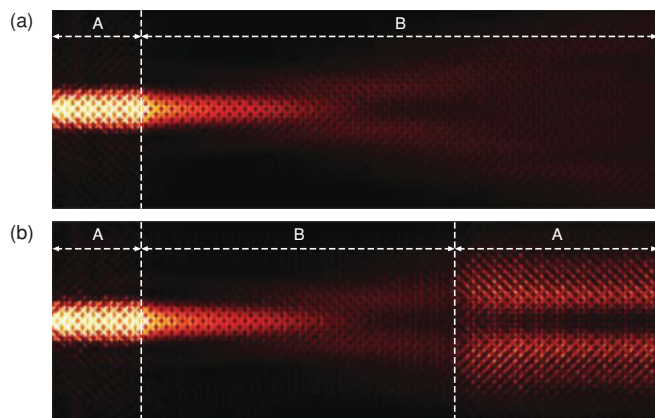


FIG. 6. (Color online) Simulated field intensity distributions at $z = 0.05a$ of the SSP beam of 15.10 GHz on a structured brass surface with (a) two different regions A and B, and (b) region B placed between the two A regions. A indicates the region where $b = 0.9a$ and B the region where $b = 0.7a$, with $h = 1.0a$ for both regions. The dashed lines indicate the interface between the two regions. The dimension of region B is $30d$ along the propagation direction in (b).

*hyPark@kaist.ac.kr

†cskee@gist.ac.kr

- ¹H. Raether, *Surface Plasmons* (Springer-Verlag, Berlin, 1988), Chap. 2.
- ²J. Saxler, J. Gómez Rivas, C. Janke, H. P. M. Pellemans, P. H. Bolívar, and H. Kurz, *Phys. Rev. B* **69**, 155427 (2004).
- ³K. Wang and D. M. Mittleman, *Nature (London)* **432**, 376 (2004).
- ⁴T. I. Jeon and D. Grischkowsky, *Appl. Phys. Lett.* **88**, 061113 (2006).
- ⁵J. B. Pendry, L. Martín-Moreno, and F. J. Garcia-Vidal, *Science* **305**, 847 (2004).
- ⁶F. J. Garcia-Vidal, L. Martín-Moreno, and J. B. Pendry, *J. Opt. A Pure Appl. Opt.* **7**, S97 (2005).
- ⁷A. P. Hibbins, B. R. Evans, and J. R. Sambles, *Science* **308**, 670 (2005).
- ⁸M. Qiu, *Opt. Express* **13**, 7583 (2005).
- ⁹F. J. García de Abajo and J. J. Sáenz, *Phys. Rev. Lett.* **95**, 233901 (2005).
- ¹⁰A. P. Hibbins, M. J. Lockyear, I. R. Hooper, and J. R. Sambles, *Phys. Rev. Lett.* **96**, 073904 (2006).
- ¹¹C. R. Williams, S. R. Andrews, S. A. Maier, A. I. Fernández-Domínguez, L. Marín-Moreno, and F. J. García-Vidal, *Nat. Photon.* **2**, 175 (2008).
- ¹²S. A. Maier, S. R. Andrews, L. Martín-Moreno, and F. J. García-Vidal, *Phys. Rev. Lett.* **97**, 176805 (2006).
- ¹³W. Zhu, A. Agrawal, and A. Nahata, *Opt. Express* **16**, 6216 (2008).
- ¹⁴A. I. Fernández-Domínguez, E. Moreno, L. Martín-Moreno, and F. J. Garcia-Vidal, *Opt. Lett.* **34**, 2063 (2009).
- ¹⁵B. K. Juluri, S.-C. S. Lin, T. R. Walker, L. Jensen, and T. J. Huang, *Opt. Express* **17**, 2997 (2009).
- ¹⁶A. I. Fernández-Domínguez, E. Moreno, L. Martín-Moreno, and F. J. García-Vidal, *Phys. Rev. B* **79**, 233104 (2009).
- ¹⁷D. Martín-Cano, M. L. Nesterov, A. I. Fernández-Domínguez, F. J. García-Vidal, L. Martín-Moreno, and E. Moreno, *Opt. Express* **18**, 754 (2010).
- ¹⁸W. Zhao, O. M. Eldaiki, R. Yang, and Z. Lu, *Opt. Express* **18**, 21498 (2010).
- ¹⁹N. Yu, Q. J. Wang, M. A. Kats, J. A. Fan, S. Khanna, L. Li, A. G. Davies, E. H. Linfield, and F. Capasso, *Nat. Mater.* **9**, 730 (2010).
- ²⁰H. Kosaka, T. Kawashima, A. Tomita, M. Notomi, T. Tamamura, T. Sato, and S. Kawakami, *Appl. Phys. Lett.* **74**, 1212 (1999).
- ²¹P. Rakich, M. Dahlem, S. Tandon, M. Ibanescu, M. Soljac, G. Petrich, J. Joannopoulos, L. A. Kolodziejski, and E. P. Ippen, *Nat. Mater.* **5**, 93 (2006).
- ²²Z. Lu, S. Shi, J. A. Murakowski, G. J. Schneider, C. A. Schuetz, and D. W. Prather, *Phys. Rev. Lett.* **96**, 173902 (2006).
- ²³V. Espinosa, V. J. Sanchez-Morcillo, K. Staliunas, I. Pérez-Arjona, and J. Redondo, *Phys. Rev. B* **76**, 140302 (2007).
- ²⁴E. Soliveres, V. Espinosa, I. Pérez-Arjona, V. J. Sánchez-Morcillo, and K. Staliunas, *Appl. Phys. Lett.* **94**, 164101 (2009).
- ²⁵S. S. Oh, S.-G. Lee, J.-E. Kim, and H. Y. Park, *Opt. Express* **15**, 1205 (2007).
- ²⁶A. Taflov and S. C. Hagness, *Computational Electrodynamics: The Finite-Difference Time-Domain Method*, 2nd ed. (Artech, Norwood, 2000).